Improved Bi-Spectral Method for Mapping Insolation Using NOAA APT Images

Md. Rafiqul Islam
Assistant Professor
Department of Mechanical Engineering
Bangladesh Institute of Technology, Khulna
Khulna-9203, Bangladesh

and

R.H.B. Exell
Professor, Department of Mathematics
King Mongkut's Institute of Technology. Thonburi
Bangmod, Rasburana, Bangkok 10140, Thailand

ABSTRACT

An operational low cost system for mapping daily and monthly global solar radiation reaching the ground over a geographical area of 13" latitude by 8° longitude using NOAA APT images has been developed for use in south and southeast Asia. An improved statistical bi-spectral model is used with visible and far infrared APT images to calculate the cloudiness of targets of size 111 km by 111 km. One to three measurements in a day by NOAA satellites are combined with variable weights to calculate the effective cloudiness for the whole day. Ground measured radiation data from selected stations within the area covered are then correlated with the calculated cloudiness. Solar radiation can be estimated over the land and over the ocean equally well using the improved model. The standard error of estimation of daily global radiation is in the range 6-19% of the measured mean.

1. INTRODUCTION

There is no routine solar radiation mapping system for the developing and underdeveloped countries in south and southeast Asia to support the radiation database useful for solar energy. agricultural, meteorological, environmental and other applications. Widely spread networks of pyranometers for mapping solar radiation over large areas are still rare even in developed countries because of the very high cost. Use of meteorological satellite data for estimating solar radiation at the ground developed after the inclusion of radiometers in the payload of TIROS satellites in 1960. Different methodologies were developed for this purpose using different types of images from different satellites. Recently operational and real-time mapping of solar radiation using geostationary satellites has been successfully demonstrated [1,2]. However, the cost of these techniques is still high so they are not affordable by the developing and underdeveloped countries. The development of a low cost system for the operational mapping of solar radiation using low cost images and small computers was, consequently, the prime objective of this study as proposed by Exell and Islam [3].

The system we developed and installed at the Asian Institute of Technology (AIT), Bangkok, uses low resolution APT images transmitted from NOAA polar orbiting satellites. The hardware system comprises a low cost NOAA APT image receiver WSR524 with a small non-tracking antenna manufactured by Feedback Instruments, England, connected through an interface card to a general purpose personal computer with monochrome monitors. The system requires a 40 Mbyte hard disk in the computer, and the output can be stored on ordinary diskettes. The cost of this system did not exceed US$ 11,000 in 1990.

The image produced by the receiver has only sixteen grey levels (0-15) and its ground resolution is 6.6km by 10.8km. The effective mapping coverage can be as large as 15° latitude and 20° longitude near the equator. Three image acquisitions are taken from the morning, afternoon and evening passes (nominally 07:30h, 14:30h and 19:30h) of two NOAA satellites. The infrared data (channel4 of AVHRR, 10.5-11.5μm) from all these passes are used to obtain cloud cover, and the so-called visible data (actually the near infrared band 0.725-1.1μm, channel-2 of AVHRR) from only the afternoon pass are used to calculate cloud optical thickness. One to three measurements in a day are combined with variable weights to calculate daily effective cloudiness. Solar radiation can be estimated over the ocean and over the land equally well using our model.

An operational software package, RADMAP, has been developed to perform all tasks in simple interactive modes starting from image recording through subsequent processing of satellite and ground data to produce the final output in different media.

1.1 Study Area, Study Period and Radiation Measuring Stations

The experiment takes a mapping area covering most of Thailand and some parts of the neighboring countries, with the image receiving station nearly at the center. The areal coverage and solar radiation measuring stations are shown in Fig. 1. The map size was 1,443 km by 888 km consisting of 104 targets of size 111km by 111km. The one year study period extends from October 1991 to September 1992. It was not possible to gather solar radiation data from Cambodia or Vietnam, or from the southwest part of Thailand.

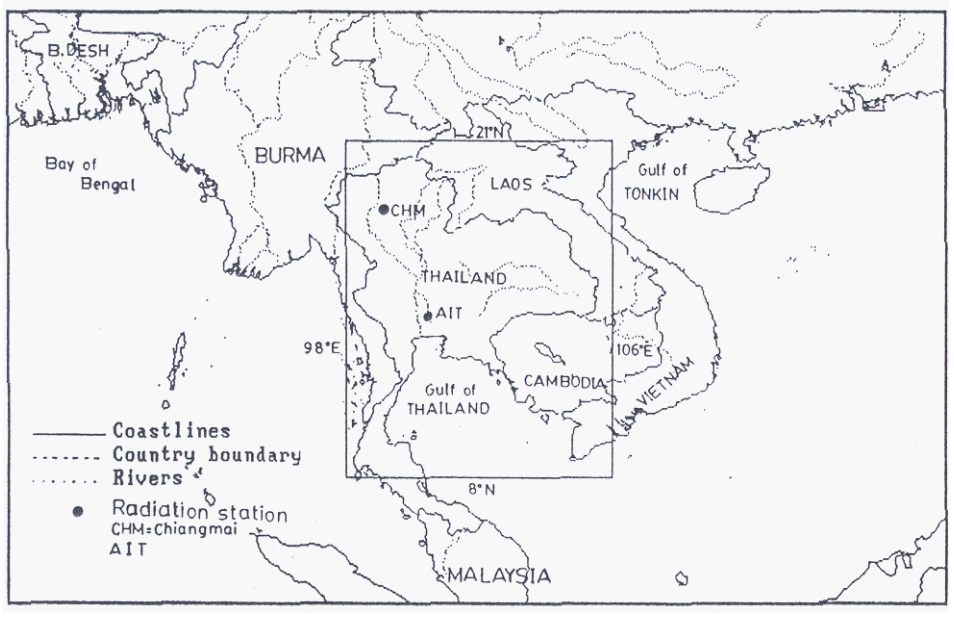

Fig. 1. Geographical coverage and radiation measuring stations of the study area.

2. THE IMPROVED BI-SPECTRAL METHOD

The bi-spectral method developed by Sorapipatana [1] gave good results using high resolution GMS HRFAX images but could not estimate solar radiation over the ocean. The following improvements and modifications were required to achieve the present objectives with our low cost system.

1. The concepts of the model were reformulated in such a way that solar radiation could be estimated over the ocean as well as over the land.
2. The algorithms were modified so that cloud cover and cloud optical thickness could be extracted independently from the infrared and visible images respectively. These algorithms are insensitive to noise, including the noise at the time of image reception with the low cost receiver.
3. A separate algorithm rejects extremely noisy data. This algorithm is not described in this paper but can be seen in [4].
4. Daily effective cloudiness is estimated from a varying number of satellite passes (1 to 3) depending on the available data.

2.1 Cloudiness Factor

Because this work is done for solar energy applications cloudiness is defined here as the amount of solar energy that cannot reach the ground surface due to the presence of cloud If N is the fraction of sky covered with cloud the solar radiation reaching the ground G_s is a mixture of the quantities coming through the clear part G_{cs} and the cloudy part G_{cl} as given by the following equation (1).

$$G_s = (1 - N)\, G_{cs} + N G_{cl}, \quad \text{or} \quad G_s = G_{cs} + N\,(G_{cl} - G_{cs}). \tag{1}$$

The definition of cloudiness is expressed by equation (2).

$$\textit{Cloudiness} = G_{cs} - G_s, \quad \text{or} \quad \textit{Cloudiness} = N\,(G_{cs} - G_{cl}). \tag{2}$$

If G_o is the extraterrestrial solar radiation incident at the top of the atmosphere and A_s is the ground albedo, the energy conservation equation can be written:

$$G_o = G_a + G_r + G_s(1 - A_s), \quad \text{or} \quad G_s = (G_o - G_a - G_r)/(1 - A_s), \tag{3}$$

where G_a is the solar radiation absorbed by the atmosphere, and G_r is the reflected solar radiation seen by the satellite (see Fig.2).

We now have the following energy conservation equations (4) and (5) for clear and overcast cloudy skies, respectively:

$$G_{cs} = (G_o - G_{acs} - G_{rcs})/(1 - A_s), \tag{4}$$

$$G_{cl} = (G_o - G_{acl} - G_{rcl})/(1 - A_s). \tag{5}$$

In a short period of time the variation of A, is neglected. Cloud is the first order attenuator of solar radiation and the attenuation by atmospheric constituents (aerosols, water vapour and other gas

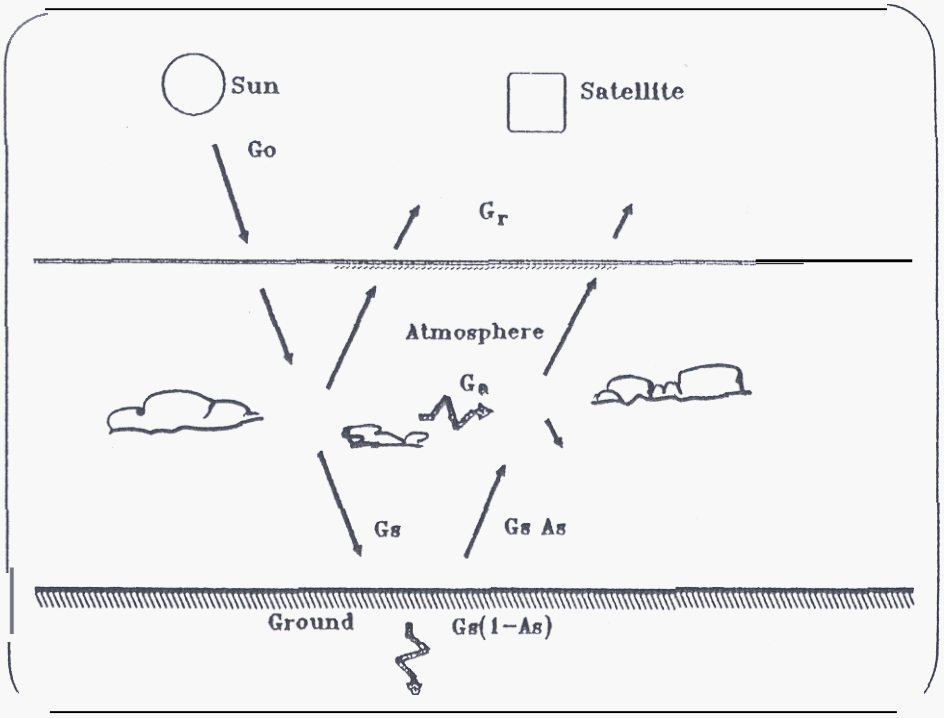

Fig, 2. Passage of solar radiation flux densities in shortwave range from the Sun to satellite through the Earth-atmosphere.

molecules) are of second order [5, 6 and 7]. The absorption in the atmosphere is assumed to be mainly due to water vapor. Absorption in the cloud is very low.

The water vapor content of the atmosphere when the sky is cloudy is expected to be greater than the water vapour content when the sky is clear. However, in a cloudy sky the water vapour content above the cloud is negligible compared with the amount below the cloud [8], but the intensity of solar radiation interacting with the water vapour below the cloud is less than that of solar radiation in a clear sky. Consequently, we assume there is negligible difference in total atmospheric absorption between cloudy and clear sky conditions, i.e. $G_a = G_{acl} = G_{acl}$. This assumption is consistent with Dedieu [9], who also assumed no molecular scattering and absorption under a cloudy sky.

With above assumptions, and using equations (4) and (5) to substitute for G_{cs} and G_{cl} in equation (2), we obtain equation (6) for the cloudiness:

$$\textit{Cloudiness} = N\,(G_{rcl} - G_{rcs}) / (1 - A_s). \tag{6}$$

Finally, we define a dimensionless ***cloudinessfactor C***:

$$C = (\textit{Cloudiness})\,(1 - A_s) / G_o = N\,(G_{rcl} - G_{rcs}) / G_o = N\,(A_{cl} - A_{cs}) \tag{7}$$

where A_{cl} is the albedo of the overcast cloud top including the atmosphere above the cloud, defined by $A_{cl} = G_{rcl}/G_o$, and A_{cs} is the albedo of the clear sky planet (atmosphere & surface), defined by $A_{cs} = G_{rcs}/G_o$.

The cloudiness factor C can also be interpreted as the "***lost transmittance***" of the clear sky atmosphere due to the presence of cloud.

2.2 Atmospheric Transmissivity for Solar Radiation

The transmissivity T of an atmospheric column is defined as the ratio of the solar energy reaching the ground through the column to the extraterrestrial solar radiation incident at the top of the column:

$$T = G_s / G_o \tag{8}$$

2 3 Cloudiness Factor Correlated with Atmospheric Transmissivity

Replacing G_{cl} and G_{cs} in equation (1) using equations (4) and (5) and the assumptions made in Section 2.1 we obtain

$$G_s = (G_o - G_{acs} - G_{rcs}) / (1 - A_s) + N (G_{rcs} - G_{rcl}) / (1 - A_s)$$

Dividing both sides of the above equation by G_o, assuming G_{acs} equals G_a, and inserting T from equation (8), we obtain

$$T = a + b C, \tag{9}$$

where $a = (1 - G_a / G_o - A_{cl}) / (1 - A_s)$, and $b = -1 / (1 - A_s)$.

Now, if the quantities a and b are assumed constant over a period of about one month, the present model is a simple linear expression correlating the cloudiness factor from satellite images with atmospheric transmissivity from measurements of solar radiation at the ground. The following expression can then be used for estimating solar radiation reaching the ground at desired targets from satellite images:

$$G_s = G_o (a + b C) \tag{10}$$

2.4 Justification of the Assumption that a and b are Constant

The surface albedo A, is a function of surface properties which may remain stable for a short period of time (eg. one month). However, it varies more over green vegetation and ordinary land than over Oceans and desert areas when measured in the visible channel. For a fixed geographical location and a sufficiently large target (1° x 1°) this variation is not noticeable over short periods in the APT images.

Nunez [10] found that variations of water vapor and aerosol absorption are more important in the depletion of solar radiation in a clear sky than other processes, but still he assumed absorption and scattering to be constant over time. In physical models ([8] and [9]) or in some empirical models ([11] and [12]) the absorption and scattering properties are obtained indirectly from measurable quantities like surface pressure, vapor pressure, thickness of precipitable water vapor (cm), depth of aerosols or mixed gases, etc, [13]. According to Vonder Haar and Ellis [12], empirical relations which express absorption (or scattering) as a function of these measurable quantities may still show notable scatter. An r.m.s. scattering of about 9% (or 1.76 MJ/m²d) in calculating absorbed energy from water vapor optical depth (cm) was mentioned by Vonder Haar and Ellis [12]. Thus, attempts to improve the model in this way are not worthwhile.

Furthermore, if calculated values of absorptivities and reflectivities are to be introduced in the formulation, the system will depend on the ancillary climatological data. In this region, such data are

m e and timely availability on a continuous basis cannot be ensured. Moser and Raschke [5 and 6] avoided the use of these quantities to make the physical model simple. Tarpley [14] concluded that ancillary data do not have any effective and economic contribution to the accuracy of estimation of atmospheric transmissivity obtainable from satellite data.

If in clear skies there are any changes in the absorption during the downward or upward passage of solar radiation, the planetary reflectivity also changes in the opposite direction. Therefore, the coefficienta is stabilized by counterbalancing these two components of a. This is also evident in the results of Sorapipatana [1], who found a more stable than the second coefficient of his model, which contains no term that counterbalances the variation of clear sky planetary albedo in it's numerator.

Therefore, the coefficients a and b are assumed constant over one month periods to make the operational system easy, simple and economic without losing a significant amount of accuracy of estimation.

2.5 The Fractional Cloud Cover, N

Consider the thermal radiation in a vertical column of the atmosphere at a pixel i of the image. The walls of this column are in equilibrium with the surrounding atmosphere. Thermal radiation from the ground, the atmosphere and cloud is emitted from the column through the top and is measured by the satellite sensor.

Suppose the pixel contains some cloud, whose thermal infrared radiance including the emission from the atmosphere above the cloud is I_{cl}, covering a fraction N_i of the pixel area. The thermal infrared radiance of the clear part of the sky also including all the atmosphere above the ground is I_{cs}. Now, the radiance measured at the sensor for the pixel is the equivalent radiance emitted from the whole pixel I_i, which can be written as:

$$I_i = I_{cl}N_i + I_{cs}(1 - N_i),$$

which gives

$$N_i = (I_i - I_{cs}) / (I_{cl} - I_{cs}). \tag{11}$$

When a target area consists of m pixels, the target cloud cover fraction can be expressed as:

$$N = (1/m) \sum_{i=m}^{m} N_i \quad \text{or} \quad N = (I_m - I_{cs}) / (I_{cl} - I_{cs}), \tag{12}$$

where I_m is the target mean radiance.

Even though different types of cloud may occur, or one cloud type may not fully fill one pixel, equation (12) assumes that one type of cloud is present in the target whose radiance is equivalent to the effective radiance from different types of cloud, and the clear sky radiance is the equivalent radiance from different types of surface coverage. That is, the clear sky radiance I_{cs} and the cloudy sky radiance I_{cl} are assumed to be same in all the pixels in the target. In practice I_i is the only measurement, and to find I_{cl} and I_{cs} the pixels in the whole target have to be examined.

2.6 Cloudy Sky Parameters

The emissivity, absorptance and reflectance of the air and gas molecules, and the temperature profile of the atmosphere above the cloud, can be considered very stable when compared with the variation of these properties due to the enormous variety of clouds that may occur. Thus, the cloudy sky parameters are assumed to be mainly dominated by cloud properties.

A pixel containing broken cloud patches at any level may emit the same radiance as a pixel fully covered with low level warm clouds. In general, the same radiance may be obtained from varying cloud fractions and clouds of varying emissivity and temperature (height). So the parameters A, I_{cl} and N become interdependent, especially in a low resolution image.

If a pixel has radiance smaller than the target mean radiance, Smith [15] identified the pixel as a cloud contaminated pixel. He calculated I_{cl} as the mean radiance of these cloud contaminated pixels. Sorapipatana [1] simplified Smith's algorithm by calculating cloud radiance as one standard deviation less than the target mean radiance after assuming pixels are normally distributed about the mean and the maximum error would be 6.12% for real situations. But it is shown by one of us (Islam [4]) that the cloud radiance should be the mean radiance minus 4/5th of one standard deviation. The standard deviation serves as an indicator of the presence of cloud in Sorapipatana's method. This approach is inapplicable for images having unusual noise as in our low cost system.

In our method, which is described in the following sections, we assume three main types of cloud: low, middle and high clouds, and the frequency histogram of grey levels in the whole target is used to give an idea of the distribution of possible cluster centers in each band.

2.6.1 Pseudo Cloud and Cloudy Sky Radiance, I,,

Given a multi-modal histogram, each class center can be located at respective modes from the histogram. We calculate cloud radiance I_{cl} as the mode at the cold side of the thermal infrared histogram. This mode is chosen as the apparent cloud radiance of the target. But, to make statistically accurate calculations and to fit the actual situation, we merge possible cloud types into one type by calling it a "pseudo cloud.

The pseudo cloud radiance is calculated as the weighted mean of the three coldest modes (for three cloud types, if they exist) whose radiance is less than the target mean radiance.

In nearly clear sky situations there may not be any peaks on the cold side of the histogram. In such cases we assume as pseudo clouds the most recent cloud type (not older than one month) for the particular geographic location. This assumption is justified by the known seasonal persistence of cloud types. During winter in this region cirro-stratus clouds are the most common. Alto-cumulus clouds are often seen, and nimbus or strato-cumulus clouds are rare. During summer, low clouds, middle clouds and cumulo-nimbus clouds are most likely.

2.6.2 Cloudy Sky Albedo, A ,

The pseudo cloud concept is also applied in calculating the cloud albedo from the visible channel. To overcome the difficulties in calculating the cloudiness factor due to the effects of different types of cloud in the target, the cloud albedo A_{cl} is simply assumed to be the mean albedo of all the pixels having brightness greater than the clear sky albedo of the target:

$$A_{cl} = (1/k) \sum_{i=1}^{m} A_i \qquad (13)$$

where, $A_i = A_i$ for $A_i > A_{cs}$, and the pixel is considered to be cloud contaminated,
$A_i = 0$ for $A_i \leq A_{cs}$, and the pixel is considered to be cloud free,
k = number of cloud contaminated pixels,
m = number of pixels in the target.

2.7 Clear Sky Parameters

Sorapipatana [1] selected as clear sky infrared radiance the modal peak on the high radiance side of the infrared grey level histogram over the target from a set of images whose standard deviation over the target was lower than a certain threshold. The visible grey level histogram of the pixels in these targets has a low brightness peak which was taken to be the clear sky brightness (or albedo), and a high brightness peak, which was taken to be caused by low cloud.

Because clouds are non-stationary, D. Cano et al., [16] used the minimum albedo of a pixel from a number of images taken over a period of time as the clear sky visible albedo.

In our system, targets are large and may contain different surface features, so the clear sky parameters for a target are the mean values for all types of surface in the target. The principle types of surface are land surfaces and Ocean surfaces, but many of the targets contain both types.

The following subsections state how the clear sky parameters are found in our method.

2.7.1 Clear Sky Infrared Radiance, I_{ci}

The infrared image histogram of the target is plotted and modes are identified. The modes with the highest radiance are obviously from clear sky or from very low level warm clouds. The weighted mean of the two modes (for two surface classes, if they exist) which are greater than the target mean radiance is stored as the provisional clear sky radiance of the target for the time of measurement in the day. The minimum from these provisional clear sky radiances for a period of one month is considered to be the true clear sky radiance of the target I_{ci}.

2.7.2 Clear Sky Planetary Albedo, A_{ci}

We first calculate the weighted mean of the lowest two modes which are on the low brightness side of the visible histogram for the target and which are lower than the target mean brightness. These values are stored for one month periods and the minimum of these data sets is taken as the clear sky planetary albedo over the target. The reason for taking two low brightness modes is that there may be both land and ocean surfaces in the target area. Difficulties caused by snow or white sandy desserts do not occur in the study area.

2.8 Daily Effective Cloudiness from Multiple Measurements in a Day

Sorapipatana [1], Nunez [10] and Tarpley [14] took simple arithmetic averages of all cloudiness measurements in a day at asymmetric hours from noon to obtain daily effective cloudiness.

At any particular location the same level of cloudiness will obstruct more solar energy at noon than at other times. So when two or more satellite measurements at different times are used to calculate daily effective cloudiness different weights should be given to these measurements. Fixed weights cannot be used when satellite acquisition times vary due to orbital perturbations. Therefore variable weights are used in multivariable linear correlations between daily mean values of T and values of C at different times of the day as explained in the following sections.

2.8.1 General Model Expression

Let C_m, C_a and C_e be the cloudiness estimates in the morning, afternoon and evening, respectively. Then:

$$C_m = N_m (A_{cl} - A_{cs}),\ C_a = N_a (A_{cl} - A_{cs}),\ \text{and}\ C_e = N_e (A_{cl} - A_{cs}),$$

where the N's are the fractional cloud covers obtained from infrared images. The quantities A_{cs} and A_{cl} are obtained only from the afternoon visible image. Let W_m, W_a and W_e be the respective weights for each cloudiness. Then the daily effective cloudiness factor C is written in the form

$$C = W_m C_m + W_a C_a + W_e C \qquad (14)$$

where, $W_m + W_a + W_e = 1$.

2.82 Fitting Data to the Model Expressions

The model actually used is based on equation (9), Section 2.3, and (14) above. According to the availability of cloudiness data, four possible types of model are generated:

Type (1): only afternoon: $T = a + b C_a$
Type (3): afternoon and evening: $T = a + b_a C_a + b_e C_e$
Type (5): afternoon and morning: $T = a + b_a C_a + b_m C_m$
Type (7): afternoon, morning and evening: $T = a + b_m C_m + b_a C_a + b_e C_e$.

(These types are labeled by odd numbers in accordance with the coding used in the computer software.)

Now, the weights can be calculated from the coefficients as follows:

Type (3): $b = b_a + b$, and $W_a = b_a/b$ and $W_e = b_e/b$
Type (5): $b = b_a + b_m$, and $W_a = b_a/b$ and $W_m = b_m/b$
Type (7): $b = b_m + b_a + b_e$, and $W_m = b_m/b$, $W_a = b_a/b$ and $W_e = b_e/b$.

3. OPERATIONAL METHODOLOGY

3.1 Navigation

The geographical target points are located on the image using a procedure called navigation. The procedure follows three steps (1) NOAA-AVHRR coordinates are generated using orbital models similar to Brush [17] with some simplification, (2) NOAA-AVHRR Coordinates are mapped to NOAA-APT coordinates, and (3) NOAA-APT coordinates are mapped to WSR524 image coordinates.

The concepts of a Keplerian orbit were assumed, and the published nominal satellite attitude and sensor parameters were used. The ellipsoidal shape of the earth was considered but the nutation of the earth's axis and the movement of the equinoxes were omitted. Brouwer mean orbital parameters from Part IV of the teletype bulletin US (TBUS) were taken. The r.m.s. error of navigation was 1.06 pixels along, and 2.24 pixels across, the satellite nadir track. This was reduced to within one pixel by manual correction using ground control points.

3.2 Calibration

The calibration published by NOAA for converting visible image data from grey levels to albedo was not used since our images have passed through a contrast enhancement procedure in the receiver. However, the visible data were normalized by dividing by the cosine of the solar zenith angle. The calibration of infrared data was not required for the equation (12) since linear conversion functions are assumed to calculate radiance from grey values [18].

3.3 Updating of the Model

The first set of model coefficients was obtained from the data period October to December 1991. The next update of the model coefficients was performed in February 1992 by replacing the oldest data with the newest data. This was followed by updating at one month intervals.

3.4 Radiation Mapping

Cloudiness factors for the moming, aftemoon and evening were calculated according to the availability of satellite data for all targets of the map. The model coefficients of the model type having the least standard error between the atmospheric transmissivity T as determined by measurement on the ground and the values estimated by the model from satellite data at a station nearest to the target were used to calculate the daily effective cloudiness factor by equation (14) at all targets of the map. This was then used to calculate the daily total global solar radiation using equation (10) at all targets of the map.

4. RESULT AND DISCUSSIONS

Table 1 summarizes, as an example, the model coefficients updated in February 1992. Figures 3 and 4 give regression plots for the model type 1 from Chiang Mai and AIT, respectively, for the same month. Tables 2 and 3 give standard errors of estimate of daily radiation for the whole period. The mean standard error of estimation was 12.9% with a range of 6%-19% of the measured mean for daily total global solar radiation at the ground. Table 4 gives the bias errors and the r.m.s. errors of estimation in monthly mean radiation, which were 1.29 MJ/m²d at Chiang Mai and 1.46 MJ/m²d at AIT. Figure 5 presents the grey scale maps of monthly mean radiation and monthly natural variability (coefficient of variation) of radiation in February 1992.

To find the actual error of estimation of daily global solar radiation two tests have been performed. Model coefficients for Chiang Mai were used to estimate the radiation at AIT in the first test for the period January to April 1992. In the second test, the models for AIT were used to estimate the radiation at Chiang Mai for the same period. When estimated daily global solar radiation values are compared with ground measured values, the mean r.m.s. error of estimation from these two tests was 14.45% of the measured mean. Figure 6 shows the comparison between estimated and measured radiation values.

Among the sources of inaccuracy in estimating solar radiation using the present system the following may be mentioned: the use of a large target area, imperfection in detecting and removing reception-time interference from the image, inability of the bi-spectral method to incorporate all possible real atmospheric effects perfectly, defects in the ground measured radiation data used for

Table 1. Model coefficients for February 1992

General Expression: T = a + baCa + beCe + bmCm
Yerr = standard error 100 = insufficient data
Month of Update: Feb '92 Data Period: 9112-9202
R=Correlation coefficient
Df = Degree of Freedom

Model Identity	a	ba	be	bm	R	Yerr	YErr%	Df
ChiangMai								
Type 1	0.688649	-1.34627	0	0	0.819332	0.070545	12.32	32
W's		1	0	0	b =	-1.34627		
t-ratio	38.703	-8.084						
Type 3	0.749363	-1.32158	-1.51593	0	0.910922	0.063246	11.5	12
W's		0.465754	0.534245	0	b =	-2.83751		
t-ratio	20.963	-1.807	-1.617					
Type 5	0.670744	-0.36718	0	-0.90229	0.768442	0.060074	10.2	14
W's		0.269232	0	0.710767	b =	-1.26945		
t-ratio	21.169	-0.717		-2.379				
Type 7	0.717045	-0.36468	-1.64761	-0.26693	0.872893	0.076217	13.39	4
W's		0.160002	0.722883	0.117114	b =	-2.27922		
t-ratio	10.76	-0.235	-0.696	-0.317				
AIT								
Type 1	0.575467	-0.75427	0	0	0.706432	0.069518	13.32	65
W's		1	0	0	b =	-0.75427		
t-ratio	53.318	-8.047						
Type 3	0.595231	-0.58087	-0.20086	0	0.897553	0.057127	11.74	7
W's		0.743053	0.256946	0	b =	-0.78174		
t-ratio	21.899	-0.539	-0.194					
Type 5	0.573071	-0.59320	0	-0.06177	0.778972	0.059758	11.69	29
W's		0.905691	0	0.094308	b =	-0.65497		
t-ratio	39.218	3.685		-0.289				
Type 7	0.622781	-0.28644	-0.09323	-0.71326	0.962466	0.040881	8.79	4
W's		0.262083	0.085303	0.652612	b =	-1.09294		
t-ratio	20.142	-0.488	-0.156	-1.998				

Note: Model type definitions are given in the text

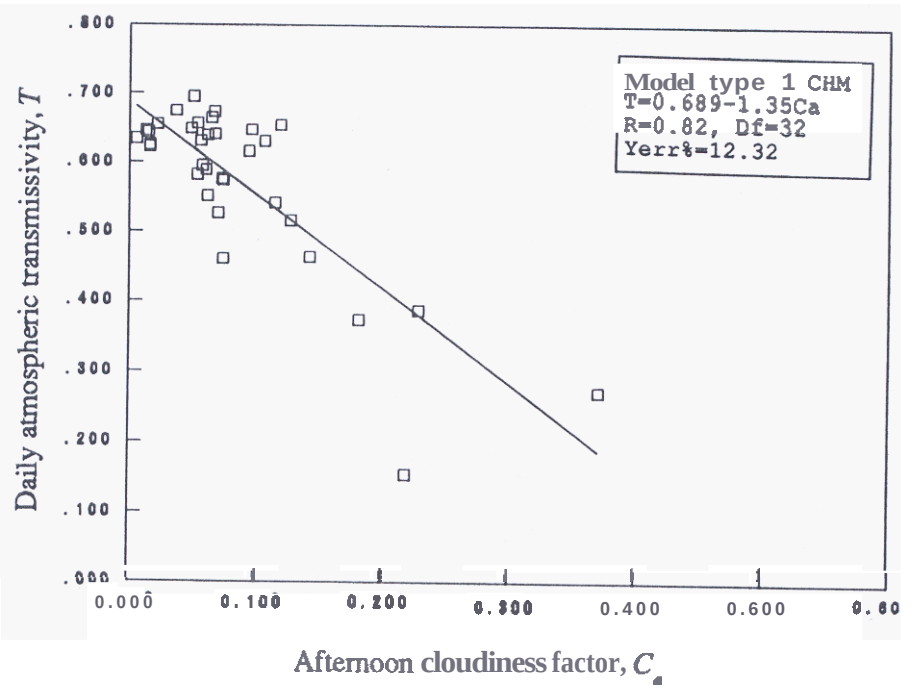

Fig. 3. Regression plot for model type 1 at Chiang Mai in February 1992.

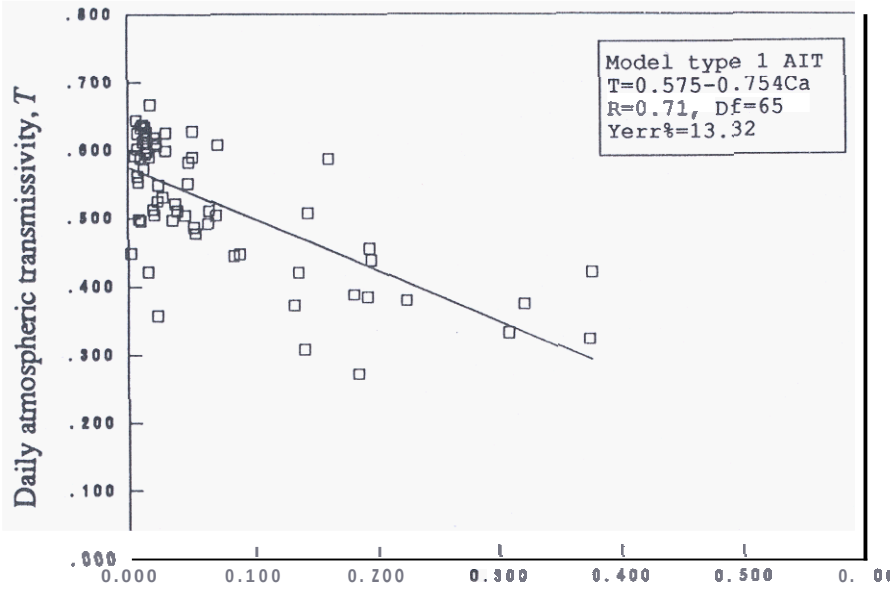

Fig. 4. Regression plot for model type. 1 at AIT in February 1992.

Table 2. Standard errors of estimate of daily global solar radiation (%) according to station.

Period	ChiangMai			AIT			All Stations		
	Max	Mean	Min	Max	Mean	Min	Max	Mean	Min
9112	13.17	13.17	13.17	10.74	9.82	7.21	13.17	11.49	7.21
9202	12.32	11.34	10.20	13.32	11.39	8.79	13.32	11.36	8.79
9203	14.00	12.54	11.08	13.48	12.22	10.31	14.00	12.38	10.31
9204	10.99	8.52	6.05	12.69	11.13	10.21	12.69	9.83	6.05
9205	11.26	10.49	9.72	11.13	11.05	10.96	11.26	10.77	9.72
9206	13.65	13.65	13.65	12.37	12.21	12.04	13.65	12.93	12.04
9207	17.17	15.41	13.65	17.55	16.12	14.69	17.55	15.77	13.65
9208	17.28	15.55	13.81	18.33	16.02	14.36	18.33	15.78	13.81
9209	18.61	15.19	13.34	19.05	16.30	14.47	19.05	15.75	13.34
All Period	18.61	12.87	6.05	19.05	12.92	7.21	19.05	12.89	6.05

Table 3. Standard errors of estimate of daily global solar radiation (%) according to model type.

Model Type	ChiangMai			AIT			All Stations		
	Max	Mean	Min	Max	Mean	Min	Max	Mean	Min
1 (A)	18.61	14.27	10.99	19.05	14.22	10.75	19.05	14.25	10.75
3 (AE)	18.52	13.86	6.05	23.85	17.06	11.74	23.85	15.46	6.05
5 (AM)	18.20	12.76	9.72	14.69	12.13	10.22	18.20	12.45	9.72
7 (AEM)	13.39	13.39	13.39	15.38	10.47	7.22	15.38	11.93	7.22

Table 4. Estimated and measured monthly mean of daily global solar radiations (MJ/m²).

Month	ChiangMai Estimated	ChiangMai Measured	ChiangMai Bias	AIT Estimated	AIT Measured	AIT Bias
Oct 91	16.11	-	-	13.3	14.77	-1.47
Nov 91	17.1	-	-	16.7	16.69	0.01
Dec 91	16.02	14.16	1.86	15.4	15.47	-0.07
Jan 92	15.13	16.53	-1.4	14.9	15.7	-0.8
Feb 92	19.75	17.7	2.05	17.2	17.92	-0.72
Mar 92	21.67	19.93	1.74	19.6	20.49	-0.89
Apr 92	19.6	19.13	0.47	24.4	20.89	3.51
May92	19.37	21.1	-1.73	18.71	20.23	-1.52
Jun 92	18.63	18.27	0.36	19.02	17.8	1.22
Jul 92	15.27	14.92	0.35	18.72	17.25	1.47
Aug 92	17.32	17.79	-0.47	18.63	17.12	1.51
Sep 92	17.86	17.35	0.51	18.5	17.5	1
R.m.s. Biases (MJ/m2) =			1.29			1.46

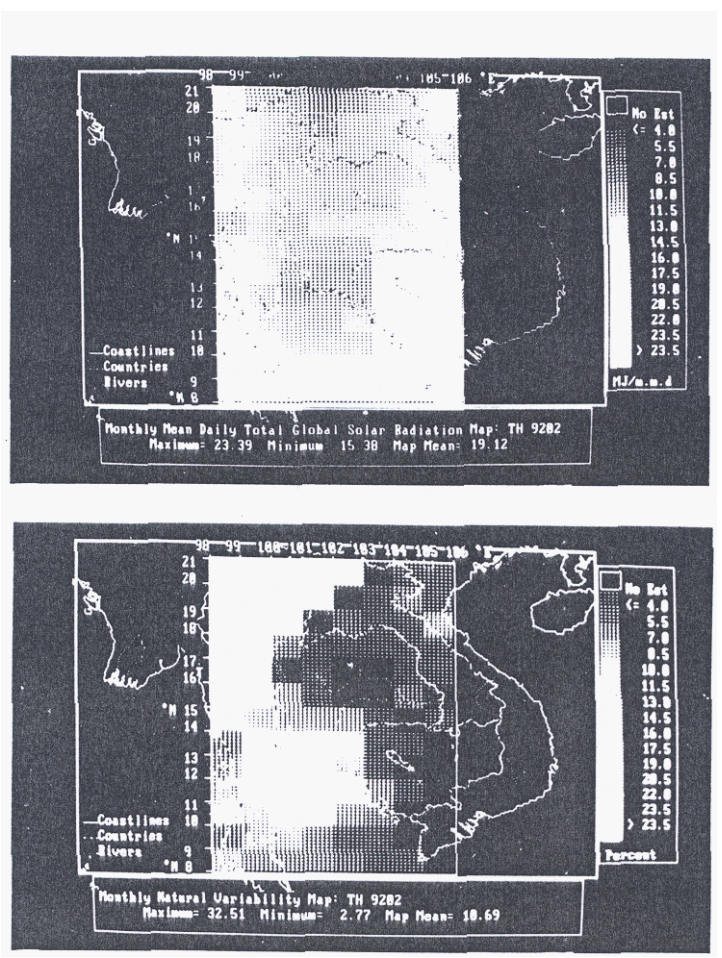

Fig. 5. Estimated radiation map (top) and the radiation variability map (bottom) for February 1992.

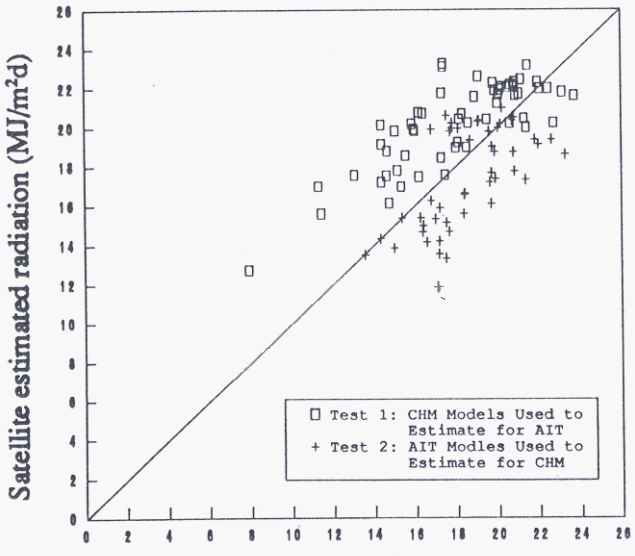

Fig. 6. Comparison between estimated and measured values of daily gloval solar radiation at the ground.

correlations, the unpredictable error in estimating radiation at one geographical target using model coefficients obtained from a distant location with different geographical terrain and surface coverage, and finally seasonal biasing induced by continuous updating of the model coefficients with past data.

However, through an analysis of the model coefficients for one year for the two radiation measuring stations it has been found that changes in the model coefficients seem to represent real climatological and geographical influences. The parameter *a* is much more stable than b. This observation is consistent with the result of Sorapipatana [1] and with the physical assumptions in our improved bi-spectral model, as discussed earlier in Section 2.

The t-ratios from the student's t-distribution and the corresponding number of degrees of freedom, and the values of Wat different times of the day in different model types for one year show that the contribution of the evening cloudiness to the daily effective cloudiness is smallest among the three measurements. The moming cloudiness measurement has a significant contribution but the afternoon cloudiness is the most important.

The correlation coefficient R between the cloudiness factor and the daily atmospheric transmissivity was always greater than 0.7.

5. CONCLUSIONS

Our new bi-spectral method gives acceptable accuracy in estimating daily global solar radiation from APT images of polar orbiting weather satellites. The method is successful with a low cost operational system to produce solar radiation maps covering a large geographical area including both land and ocean surfaces.

REFERENCES

1. Sorapipatana, C. (1988), *Mapping* Solar *Radiation Over Southeast Asia by Meteorological*

Satellite Images, D. Engg. Dissertation No. ET-88-1, AIT, Bangkok, Thailand.

2. Diabate, L., G. Moussu and L. Wald (1989), Description of An Operational Tool for Determination of Global Solar Radiation at Ground Using Geostationary Satellite Image, ***Solar Energy,*** Vol. 42, No. 13, pp. 201-207.
3. Exell, R.H.B. and Md. Rafiqul Islam (1990), Solar Radiation Mapping with a Low Cost Weather Satellite Receiver, *International Conference of Energy and Environment*, 27-30 November, 1990, Bangkok, Thailand, pp. 200-205.
4. Md. Rafiqul Islam (1993), ***Operational Mapping of Solar Radiation at the Ground Using NOAA APT Images wirh a Low Cost System,*** D. Engg. Dissertation, Energy Technology Division. Asian Institute of Technology (AIT), Bangkok, Thailand.
5. Moser, W. and E. Raschke (1983), Mapping of Global Radiation and of Cloudiness from METEOSAT Image Data - Theory and Ground Truth Comparison, ***Meteorol. Rdsch.,*** Vol. 36, pp. 33-41.
6. Moser, W. and E. Raschke (1984), Incident Solar Radiation Over Europe Estimated from METEOSAT Data, ***J. Climate and Applied Meteorology,*** Vol. 23, pp. 166-170.
7. Ferreira, M.E., E.C. Moraes, E.C. Sucharov, E.J. De Bastos, E. Raschke, R. Stuhlmann, M. Rieland and A.C. Abrahao (1991), Surface Insolation Estimates Using a Satellite Data-Based Model (IGMK) in Florianopolis, Brazil, ***Proceeding of the 24th International Symposium on Remote Sensing of Environment,*** Brazil 27-31 May 1991.
8. Gautier, C., G. Diak and S. Masse (1980), A Simple Physical Model to Estimate Incident Solar Radiation at the Surface From GOES Satellite Data, ***Journal Of Applied Meteorology,*** Vol. 19, No. 8, pp. 1005-1012.
9. Dedieu, G., P.Y. Deschamps and Y.H. Kerr (1987). Satellite Estimation of Solar Irradiance at the Surface of the Earth and of Surface Albedo Using a Physical Model Applied to METEOSAT Data, ***J. Climate and Applied Meteorology,*** Vol. 26, No.1, pp.79-87.
10. Nunez, M. (1984). Use of Satellite Data in Regional Mapping of Solar Radiation, ***Solar World Congress,*** Edited by S.V. Szokolay, Vol. 4, pp. 2142-2147, The International Solar Energy Society Congress, Australia.
11. Davis, P.A. and G.C. Chatters (1981), Insolation Estimation with Data Derivable from Polar-Orbiting Satellite, *Summary* of ***the Workshop Sessions and Additional Papers, Satellite and Forecasting of Solar Radiation,*** pp. 53-62, Solar Radiation Division of American Section of ISES.
12. Vonder Haar, T.H. and J.S. Ellis (1978), ***Determination*** of ***the Solar Energy Microclimate of the United States Using Satellite Data,*** Final Report, NASA Grant, NAS5-22372, Colorado State University.
13. Iqbal, M. (1983), ***Introduction to Solar Radiation,*** Academic Press.
14. Tarpley, J.D. (1979). Estimating Incident Solar Radiation at the Surface from Geostationary Satellite Data, ***Journal of Applied Meteorology,*** Vol. 18, pp. 1172-1181.
15. Smith, W.L. (1970), An Iterative Method for Deducing Tropospheric Temperature and Moisture Profile from Satellite Radiation Measurements, ***Monthly Weather Review,*** Vol. 95. pp. 363-369.
16. Cano, D., J.M. Monget, M. Albuisson, H. Guillard, N. Regas and L. Wald (1986), A Method for The Determination of the Global Solar Radiation from Meteorological Satellite Data, *Solar Energy*, Vol. 37, No. 1, pp. 31-39.
17. Brush, R.J.H. (1988). The Navigation of AVHRR imagery, ***International Journal of Remote Sensing,*** Vol. 9, No. 9, pp. 491-1502.
18. Kidwell, K.B. (1991), ***NOAA Polar Orbiter Data Users Guide,*** NOAA, USA.